



Experiments and computational modelling combined to shed light on the reinforcement mechanism in reactive extruded pulp fibres/starch

Downloaded from: <https://research.chalmers.se>, 2026-04-16 05:50 UTC

Citation for the original published paper (version of record):

Sessini, V., Latty, H., Milazzo, M. et al (2025). Experiments and computational modelling combined to shed light on the reinforcement mechanism in reactive extruded pulp fibres/starch biocomposites. *Advanced Composites and Hybrid Materials*, 8(5). <http://dx.doi.org/10.1007/s42114-025-01460-5>

N.B. When citing this work, cite the original published paper.



Experiments and computational modelling combined to shed light on the reinforcement mechanism in reactive extruded pulp fibres/starch biocomposites

Valentina Sessini^{1,2} · Hélène Latty^{1,3} · Mario Milazzo⁴ · Mohsen Mirkhalaf⁵ · Giada Lo Re^{1,2,4}

Received: 4 March 2025 / Revised: 13 August 2025 / Accepted: 3 September 2025
© The Author(s) 2025

Abstract

Biodegradable and renewable biocomposites have gained interest as solutions to reduce the environmental impact of composites. In this work, pulp fibres/thermoplastic starch biocomposites were fabricated with a single-step water-assisted reactive extrusion and characterised by thermomechanical analysis. This specific manufacturing process led to a reinforcement mechanism that, through both the upper-bonding theory and traditional simulation methods, cannot be properly captured. We investigated the relevance of the interface in such phenomena through micromechanical simulations performed via full-field representative elementary volume finite elements. The deviation between the experimental and simulated results led to a deepening of the investigation of the reinforcement mechanism at the matrix/fibres interface, where the modelling hypotheses failed to describe the system. This work pioneers a joint effort between modelling and experimentation in the overarching need for theoretical descriptions of outstanding reinforced short fibre polymer composites when the interactions between polymer matrix and reinforcement exceed the ‘perfect’ adhesion of the classical micromechanics.

Keywords Interface/interphase · Tensile properties · Finite element analysis · Biocomposite engineering

✉ Giada Lo Re
giadal@chalmers.se

Valentina Sessini
sessini@chalmers.se

Hélène Latty
helene.latty@gmail.com

Mario Milazzo
mario.milazzo@unipi.it

Mohsen Mirkhalaf
mohsen.mirkhalaf@physics.gu.se

¹ Department of Industrial and Materials Science, Chalmers University of Technology, Rännvägen 2A, 41258 Gothenburg, Sweden

² Wallenberg Wood Science Centre, Chalmers University of Technology, Kemigården 4, 41258 Gothenburg, Sweden

³ National Institute of Applied Sciences (INSA) of Lyon, 20 Avenue Albert Einstein, 69621 Villeurbanne Cedex, Lyon, France

⁴ Department of Civil and Industrial Engineering, University of Pisa, L.go Lucio Lazzarino 2, 56126 Pisa, Italy

⁵ Department of Physics, University of Gothenburg, 41296 Gothenburg, Sweden

1 Introduction

Packaging residues include different materials such as metals, glass, paper, and plastics and represent most of the land-fill waste [1]. In the EU, almost 80 million tonnes of packaging waste were generated only in 2020, contributing to environmental impact awareness, which results in a strengthening of European regulations in reducing waste generation. Plastics represent 19% of such packaging wastes, mainly composed of oil-based polymers that are non-biodegradable and challenging to recycle or reuse [2].

Aiming to limit plastic waste, many efforts have been recently made to develop bio-sourced and biodegradable plastics for potentially replacing oil-based thermoplastics commonly employed in packaging and other applications [3, 4]. Bioplastics used in this framework represent 48% (almost 1.1 million tonnes) of the total bioplastics production in 2022, in which more than half are biodegradable [5]. Biodegradable plastic packaging is typically obtained from abundant and cheap renewable raw materials such as starch and cellulose, and they offer alternative end-of-life management by composting or anaerobic digestion, leading to a reduction of landfilling [6].

Starch is the prevalent raw natural material to produce biodegradable plastics because of its renewability and availability. It is, in fact, an abundant polysaccharide that is obtained from a large variety of crops at relatively low cost [7]. To use starch as a thermoplastic matrix and processed by conventional melt processing techniques as other oil-based polymers, starch needs to undergo gelatinisation, i.e. destructured in the presence of plasticisers at relatively high temperature and under shear [8]. However, its poor mechanical properties and hydrophilicity, which lead to a low water barrier, limit the employment of the so-obtained thermoplastic starch (TPS) [9]. Thus, different strategies have been applied to improve TPS performances [10]. Among them, the addition of natural fibres, such as wood pulp fibres, to reinforce TPS is an efficient approach, due to their hydrophilic character affinity with the matrix, besides their relatively low weight, high specific strength, low-cost availability, renewability, and biodegradability [11, 12]. However, the fabrication of efficient wood fibre biocomposites is challenging due to their high polarity, which leads to poor interactions with non-polar polymeric matrices, and the strong interactions between fibres due to the formation of hydrogen bonding, which hinders their effective dispersion [13]. Moreover, pulp fibres undergo hornification upon drying, making irreversible fibre–fibre agglomerations. The composite performance depends on the interface and interfacial bonding between the fibres and the polymer matrix, which must guarantee a good stress transfer to achieve good mechanical properties [14]. To address these challenges, different approaches have been employed, primarily involving the physical and chemical modification of fibre surfaces [15, 16]. This involves physical treatments such as plasma, laser, and corona treatments [17–20] as well as the chemical modification incorporating additives like surfactants and compatibilisation agents [21–23], or performing chemical reactions such as acetylation, etherification, esterification, and oxidation [24–28]. Employing these techniques helps surmount the hurdle posed by the weak interface between fibres and the matrix, which arises from the chemical polarity of fibre surfaces stemming from the abundance of polar hydroxyl groups.

Enabling an easier industrial uptake, reactive extrusion (REx) approaches for the development of fully bio-sourced and biodegradable natural fibre biocomposites are an effective strategy for achieving renewable materials and processing engineering sustainability for direct replacement of non-renewable/oil-based materials [29]. Compared with the other strategies mentioned above, reactive extrusion can be designed as a single-step processing during the manufacturing of the wood fibre biocomposites to functionalise *in situ* the fibre surface and to obtain an improved dispersion [30, 31].

Hence, through the REx, it is possible to attain both the ultimate processing of biocomposites and the surface modification of cellulosic fibres. This dual approach results in an enhanced dispersion of cellulosic fibres within the polymeric matrix and a significant enhancement in the mechanical properties of the resulting biocomposite. Furthermore, when compared to alternative techniques, REx stands out for its sustainability. It enables simultaneous fibre modification and biocomposite processing in a single step, offering economic advantages and environmental friendliness by eliminating the need for solvents.

Experimentalists are aware of the limitations of modelling when it comes to capturing the effect of an improved interface. Modelling experts use semi-empirical approaches for simulating experimental results which do not fit traditional micromechanical models. However, in the literature, theoretical approaches addressing the interface and highlighting its relevance in the reinforcement mechanism are still an open challenge.

In this work, we dig up the relationships between structure and material properties in cellulose pulp fibres/starch composites, quantified and extended from prior literature studies, by combining an experimental and computational framework for a deeper understanding of composite reinforcement. In particular, the REx of TPS/pulp fibre biocomposites in the presence of glycerol and citric acid is proposed as an effective method to efficiently plasticize native potato starch to obtain TPS and, at the same time, improve the interfacial interactions between the thermoplastic matrix and the wood pulp fibres, with the aim to boost the biocomposites' mechanical properties. The materials were wet fed in a corotation twin-screw extruder to prevent hornification of the pulp fibres upon drying [26, 32]. Computational micro-mechanical simulations are conducted to better understand the reinforcement mechanism of the developed TPS/pulp fibre biocomposites. Our work aims to deliver a micromechanical description of composites with outstanding mechanical properties, achieved through reactive extrusion, and which cannot be easily described by a classical micromechanics framework since it would consider rigid hypotheses about perfect adhesion and no slipping at the interface. Our experimental/modelling toolbox is, therefore, able to circumvent the micromechanical limitations through a dedicated simple, but effective traditional FE simulation that exploits an artefact in the description of the mechanical mechanism of composites based on specific experimental input data, without relying on computationally expensive molecular dynamics studies.

The proposed combination of the modelling and experimental demonstrates the possibility of formulating theoretical descriptions for reinforced short fibre polymer composites when the interactions between polymer matrix and

reinforcement exceed the ‘perfect’ adhesion of the classical micromechanics.

2 Materials and methods

2.1 Materials

Normal potato starch with an amylose content of about 21% was supplied by Lyckeby Stärkelsen, Kristianstad, Sweden. Glycerol and citric acid (CA) were supplied by Sigma-Aldrich (Sweden), and they were used as received. Kraft pulp was provided by Nordic Paper Seffle AB (Sweden) with 72.4 wt% of water content. The pulp was a highly beaten never-dried bleached softwood mixture of 80% spruce sulphite and 20% spruce sulphate pulp; weight fractions of cellulose, hemicellulose, and lignin were 80 wt%, 17 wt%, and 1.9 wt%, respectively, according to the carbohydrate analysis.

2.2 Reactive extrusion of TPS and its biocomposites

Starch, glycerol, deionised water, and citric acid were manually premixed in batches with a weight ratio of 100:35:60:2, following preliminary tests and previous literature [33]. Afterwards, they were stored at room temperature for 24 h to allow a greater diffusion of the plasticisers in the mixture, as well as to guarantee the water absorption into the starch granule and obtain the complete deconstruction of the crystalline structure. Moreover, following this procedure, the formation of the hydrated form of citric acid is ensured, provoking the decrease of its melting temperature from ~155 to ~10 °C [34]. The resulting mixture was processed in a co-rotating twin-screw extruder (TSE) Werner & Pfleiderer ZSK 30 M9/2 (Stuttgart, Germany), with a screw diameter of 30 mm and screw length of 966 mm, equipped with six heating zones (including the external die). The temperature profile used in the different zones was 105 °C-115 °C-125 °C-135 °C-120 °C-100 °C, operating at a screw speed of 100 rpm, and a residence time (time from the feeding of the material until reach the tip of the nozzle and exit from the die) of about 4 min. A screw design with 7 kneading elements was chosen to ensure proper mixing. The solubility of citric acid in water increases with the temperature [35]. At room temperature, citric acid is in its hydrated form, which lowers its glass transition (T_g) from 11 to -25 °C, and the melting temperature to 7 °C [34]. Therefore, we selected a

maximum extrusion temperature of 135 °C to slow the water evaporation during extrusion, crucial for starch deconstruction, and to establish a balance between hydrolysis and crosslinking reactions provoked by citric acid.

Kraft pulp biocomposites with different amounts of pulp were processed following the same procedure, changing the amount of water considering the water content of the Kraft pulp. The different formulations as well as the names of the samples are reported in Table 1.

The extruded materials were successfully compression moulded (Buscher-Guyer hydraulic press KHL 100, Zurich, Switzerland) at 130 °C, at 40 bar for 3 min and 500 bar for 1 min to obtain films from which we cut the specimens for further characterisation.

2.3 Tensile test

Tensile tests were performed on Dumbbell-shaped specimens (25 mm gauge length and 1 mm thickness) cut from compression-moulded films, after conditioning for at least 3 days at 23 °C and 53% relative humidity. A total of 3 specimens were tested for each material, with a Zwick/Z2.5 tensile tester (Zwick GmbH, Ulm, Germany) equipped with a load cell of 2 kN and at two different strain rates, which are 10 and 50 mm/min. The 10 mm/min dataset was used for benchmarking traditional models, while the 50 mm/min dataset was employed to validate the synergistic modelling approach under more dynamic conditions and enable a fair comparison with the mechanical analysis reported for similar systems in the literature. The Zwick testXpert software was used to record force and crosshead travel data. Tests were performed according to the ISO 527-2 standard. Young Modulus (E_{Young}) was obtained as the slope of the curve in the elastic region, while tensile strength (S_{break}) and elongation (ϵ_{break}) were determined at the break point.

Other characterisation methods for thermal analysis via Differential Scanning Calorimetry (DSC), thermogravimetric analysis (TGA), solubility tests, fibre length and width distribution, X-ray diffraction measurements (XRD), and Dynamic Mechanical Analysis (DMTA) are provided in the Supporting Information.

2.4 Modelling

A modelling approach was pursued to estimate the mechanical behaviour of the composites under tensile loads. At first, we used mean-field (MF) and full-field (FE)

Table 1 Compositions of the starch-based biocomposites produced

Samples	Wet TPS	TPS-P1.4	TPS-P2.8	TPS-P7	TPS-P14
Weight fraction of pulp (%)	0	1.14	2.28	5.67	11.27
Volume fraction of pulp (%)	0	1.4	2.8	7.0	13.7

approaches (both in Digimat software [36]) to obtain the mechanical response of the fabricated and tested short fibre biocomposite. The full-field approach, referred to as computational homogenisation, has been widely used for short fibre composites (see e.g. [37–40]). In this methodology, the analysis of a numerical Representative Volume Element (RVE) of a short fibre composite is conducted using numerical techniques, typically the Finite Element Method. By applying volume averaging, the homogenised material response is determined. More detailed information is available in the Supporting Information (also, in Figs. S1 and S2).

A further step to model the composite was performed by employing 3D Finite-Element (FE) models developed on COMSOL Multiphysics v. 6.2 (COMSOL Inc., Stockholm, Sweden) with materials inputs obtained from a preliminary elaboration of experimental data with traditional analytical models.

In detail, we prepared a total of five RVEs with an increasing fibre content (V_f), namely 2%, 4%, 6%, 11%, and 14% with Solidworks™ (Dassault Systèmes, Vélizy-Villacoublay, France) (Fig. 1). Fibres were modelled as askew cylinders with a maximum diameter of 0.1 mm and a maximum length equal to 0.7 mm, while the RVE was designed as a rectangular prism with dimensions of

$0.45 \times 0.4 \times 1.2$ mm. To avoid any edge effect, displacement loads were applied to additional rigid domains. Figure 1 shows three representative RVEs developed in this study.

Aiming at simplifying the FE model and to reduce the computational cost, perfect adhesion was used to model the interaction between the fibres and the matrix. Therefore, we used a linear elastic description of the materials and, to introduce the engineered functionalisation of the interface, we used an elaboration of the elastic moduli based on the V_f using experimental data with the Nielsen analytical model. This mathematical model aims at modifying the Halpin–Tsai model by considering the aspect ratio, orientation, and packaging of the filler in the matrix. The equations of the Nielsen model are the following:

$$E_c = E_m \left(\frac{1 + A\eta_N V_f}{1 - \psi\eta_N V_f} \right), \eta_N = \frac{E_f - 1}{E_m}, \psi = 1 + \left(\frac{1 - \phi_{\max}}{\phi_{\max}^2} \right) V_f \quad (1)$$

in which E_c , E_m , and E_f are the Young's moduli of the composite, the matrix, and of the filler, respectively. In addition, $A = 8.38$ and $\phi_{\max} = 0.52$ are the Nielsen coefficients for a 3D random distribution of fibres considering an aspect ratio ≈ 15 [41].

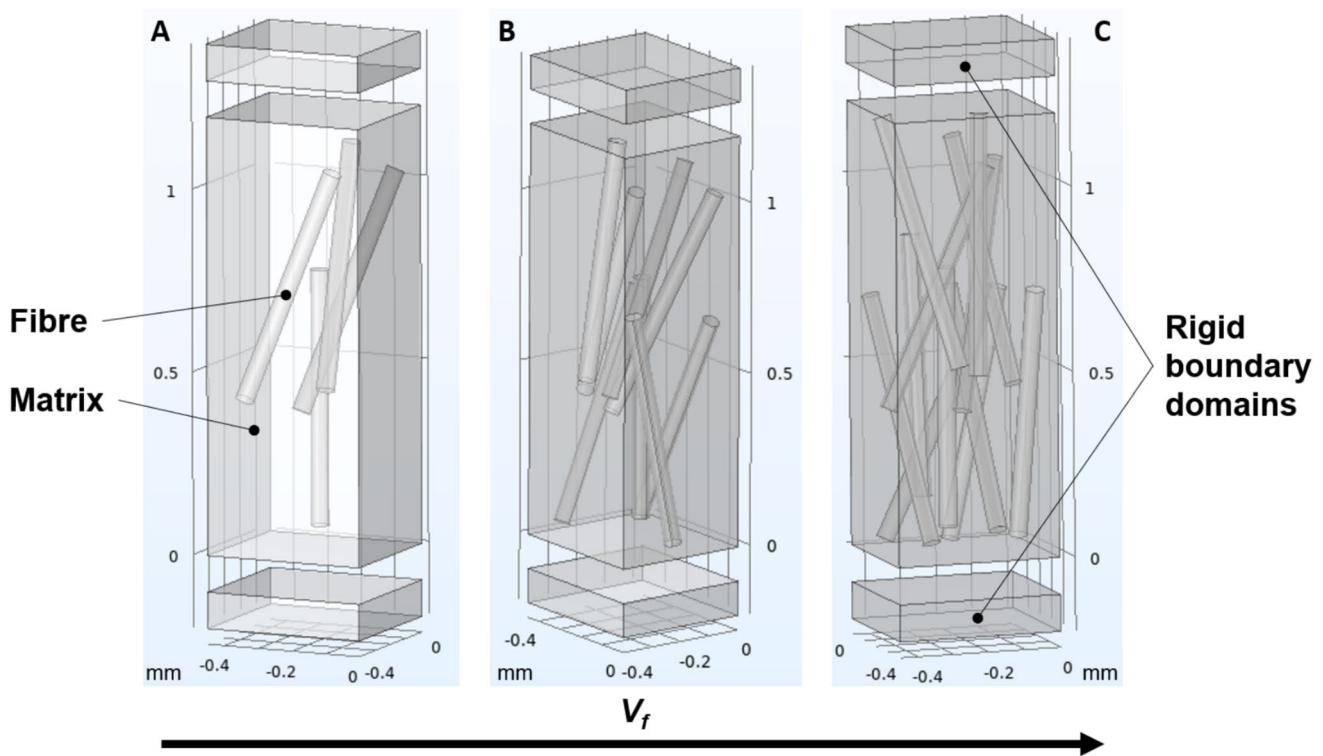


Fig. 1 Schematics of the three representative RVEs with increasing fibre content developed in the FE models. **a** $V_f=2\%$, **b** $V_f=4\%$, and **c** $V_f=6\%$

Our FE simulation approach did not employ the actual stiffnesses of the matrix and the fibres, but fictitious values (E_m^* , E_f^*):

$$E_m^* = E_{m0} \cdot f(V_f), E_f^* = E_{f0} \cdot g(V_f) \quad (2)$$

in which $E_{m0} = 251$ MPa and $E_{f0} = 40$ GPa are the actual Young's moduli of the matrix according to experimental our data and the filler according to literature [42] while $f(V_f)$ and $g(V_f)$ are two mathematical functions dependent of the volumetric fraction V_f (Eq. 3):

$$f(V_f) = a + bV_f + cV_f^2 \quad g(V_f) = d + eV_f + fV_f^2 \quad (3)$$

We combined Eq. 2, 3 with Eq. 1, and found the best analytical functions— $f(V_f)$, $g(V_f)$ —to match the experimental results of the stiffness of the composite (E_c). Eventually, the fictitious stiffness parameters (E_m^* , E_f^*) were used in a FE model that, ultimately, possessed materials with numerical values that include the mechanics of the engineered interface.

The final computational model employed tetrahedral elements with a maximum size equal to 0.025 mm and a minimum size equal to 2.5×10^{-4} mm. These element dimensions are the result of a sensitivity analysis on the obtained results. The size gradient was used to better capture the interaction between matrix and filler, with the smaller elements located at the interface.

The numerical study required a different number of elements, based on each model, according to the variation in volume fraction (V_f). As a reference, considering the model with V_f equal to 14%, the model consisted of 3,338,427 domain elements, 205,878 boundary elements, and 6353 edge elements. Tensile tests on the RVEs in the elastic range were performed to estimate the mechanical behaviour of the composite, and the Cauchy stress tensor, referred to the current deformed configuration, was used as the stress measure.

3 Results and discussion

It is well known that the crystalline structure of starch granules needs to be totally destructured to obtain homogeneous thermoplastic materials [8, 43, 44]. The crystalline structure of the native potato starch and the wet fed melt processed TPS in the twin screw extruder was investigated by XRD (Fig. S3) to verify if the destructure occurred at the processing condition chosen for the preparation of the thermoplastic starch. X-ray pattern of native potato starch displays all the characteristic peaks of the B-type structure (2θ : 5.52°, 11.18°, 15°, 17.04°, 22.93°, 26.35°, 30.90°, and 33.39°) [45–47]. The X-ray pattern of wet TPS shows that the structure of native starch granules disappeared after the melt processing, confirming that the complete granules destructure was reached at the selected processing parameters. Representative photographs (Fig. 2) show the visual aspect of the wet TPS and pulp-based biocomposite films prepared by compression moulding the TSE extrudate pellets. Transparent films were successfully obtained by the above-described procedure, even if increasing the pulp fibres content led to a darker colour.

To study the thermal transitions and the main thermo-mechanical relaxation of our systems, Dynamic Mechanical Thermal Analysis (DMTA) in tension mode (Figs. S4 and S5 and relative analysis reported in Supporting Information) was performed since the main thermal properties were not detectable by Differential Scanning Calorimetry (DSC) (Fig. S10). Our samples were characterised by multiple thermal transitions ascribed to a glycerol-rich phase, a water-plasticised starch-rich phase, and an unplasticised starch-rich phase. More detailed information is available in the Supporting Information.

For a fair comparison with the literature, the tensile properties of wet starch and its biocomposites were investigated at room temperature at 2 different strain rates:

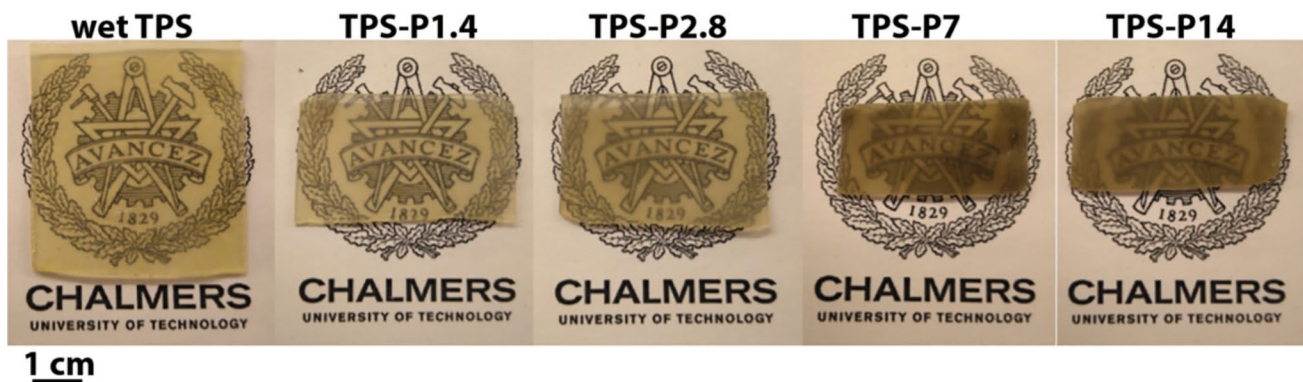


Fig. 2 Visual aspect of all the samples after melt compounding in a TSE and compression moulding. From the left to the right TPS, TPS-P1.4, TPS-P2.8, TPS-P7, and TPS-P14

10 mm/min (Fig. 3) and 50 mm/min, summarised in Table 2. The representative stress–strain curves obtained at 50 mm/min of strain rate, here not reported for the sake of brevity, showed a similar trend to the ones detected at lower strain rates.

Wet TPS showed the lowest Young’s modulus and tensile strength, but the highest elongation compared to the biocomposites. Increasing the amount of pulp fibres, the modulus and the tensile strength increase progressively, reaching maximum values of around 750 MPa and 20 MPa, respectively, for TPS-P14, 3 times higher than the values of wet TPS. Furthermore, the elongation at break decreased by more than 85% for TPS-P14 compared with that of wet TPS. As expected for viscoelastic polymers, the tests performed at higher strain rates led to higher stiffness and strength as the TPS and its biocomposites react in a more elastic way by increasing the deformation rate, lowering the systems’ relaxation time in their rubbery state.

The fibre diameter, length, and their distributions of TPS-P7 and TPS-P14 biocomposites were analysed by the Kajaani fibre analyser on fibres recovered as the insoluble fraction after Soxhlet extraction in Dimethyl Sulfoxide (DMSO) (see method description and Fig. S8 in Supporting Information). The average values of the fibre lengths decrease more than three and five times, compared to the neat pulp fibres (Table 3). The fines, referring to the fibres shorter than 0.02 mm, increase around 900% while the fibre diameter increases by about 50% compared with neat fibres. For the modelling, it was decided to use the weight average values (Table 3).

The values summarised in Table 3 highlight that, although the aspect ratio decreases as increasing the fibres amount in the biocomposites, the fines resulted from the fibrillation process generated during the reactive extrusion of the materials increase the interphase contact between fibres and matrix, leading to the enhancement of the tensile

Fig. 3 Representative stress–strain curves of wet TPS and its biocomposites obtained at 10 mm/min of strain rate testing a total of three specimens for each material

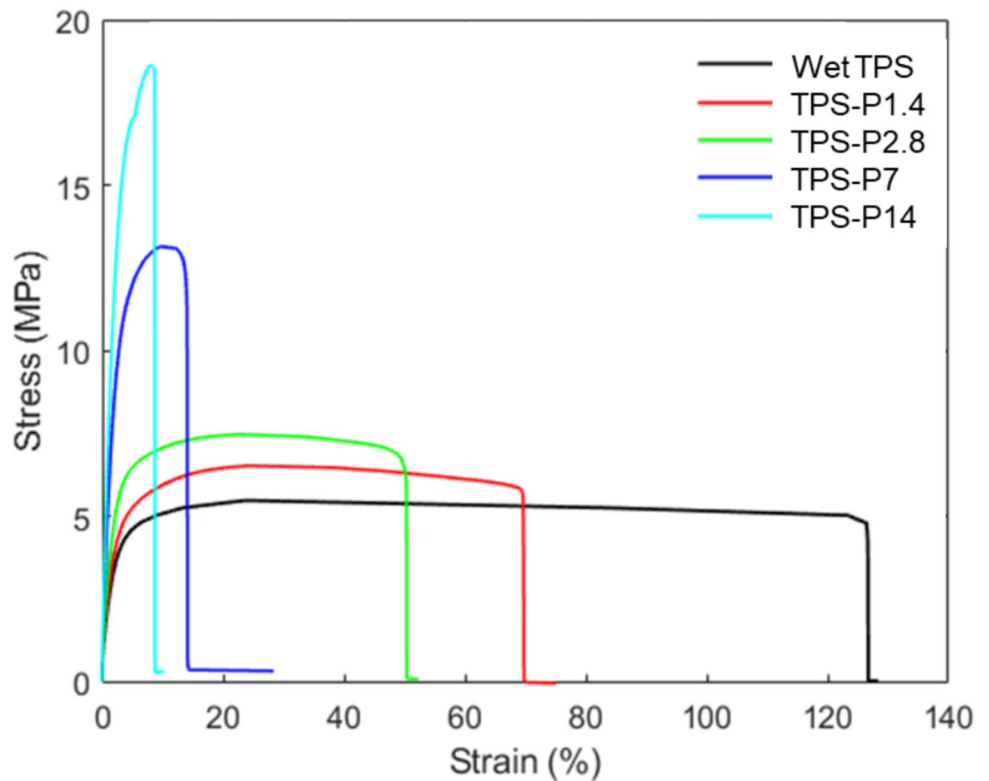


Table 2 Tensile properties of all the samples at 10 and 50 mm/min strain rates

Sample	10 mm/min			50 mm/min		
	E_{Young} (MPa)	σ_{break} (MPa)	ϵ_{break} (%)	E_{Young} (MPa)	σ_{break} (MPa)	ϵ_{break} (%)
Wet TPS	185 ± 7	6 ± 1	129 ± 6	251 ± 2	7 ± 3	76 ± 5
TPS-P1.4	197 ± 4	7 ± 1	72 ± 3	284 ± 5	8 ± 3	68 ± 9
TPS-P2.8	243 ± 1	8 ± 1	43 ± 13	360 ± 10	10 ± 2	37 ± 5
TPS-P7	364 ± 15	12 ± 2	18 ± 5	521 ± 14	15 ± 4	14 ± 2
TPS-P14	614 ± 4	18 ± 1	8 ± 3	748 ± 12	20 ± 3	9 ± 3

Table 3 Mean average values of fibre length, diameter, and fines (i.e. fibres smaller than 0.02 mm) derived from experimental data obtained by the Kajaani fibre analyser. The average values of processed fibres were applied for the modelling

Sample	Fibre length (mm)	Fibre diameter (μm)	Fines (%)	Aspect ratio (L/D)
Pristine pulp	2.77	30.4	3.5	91
TPS-P7	0.85	46.0	30.4	19
TPS-P14	0.53	47.9	35.5	11
Mean average values of processed fibres	0.69	46.9	32.9	15

properties. This result demonstrates that the REx process is essential for the mechanism of reinforcement of the pulp-fibre biocomposites. Likewise, it is important to notice that at the processing temperature, the fibre crystallinity should not be affected [21]. A decrease in the fibres crystallinity would result in a lower reinforcement effect, which is denied by the excellent mechanical reinforcement obtained by our experimental results. Hence, the enhancement of the tensile properties of the biocomposites prepared could be explained by the good adhesion between the pulp fibres and the polymeric matrix.

Therefore, scanning electron microscopy has been carried out for the TPS-P14 in comparison with the unfilled TPS (Fig. 4) to investigate their bulk morphology.

TPS cryo-fractured surface appears smooth with sporadic presence of phase-separated glycerol. In the biocomposites, the pulp fibres are well distributed and dispersed in the bulk, well embedded into the TPS matrix, and no presence of debonding or pull-outs was observed. Evidence of the fracture propagation within the fibre structure can be seen in the higher magnified micrograph (Fig. 4b'), confirming a cohesive fracture propagation typical of a system with strong interaction at the fibre-matrix interphase, consistent with the reinforcement registered in the TPS tensile properties' improvement of the biocomposites.

The experimental values of the tensile properties were compared with the values obtained with the different computational models. The traditional micromechanical mean-field (MF)/full-field (FE) modelling approaches gave lower tensile properties than those found experimentally, except for the Young's modulus calculated by MF 2D modelling at the lower fibres content (up to 7 vol.%). These results indicate that the modelling can efficiently describe or predict the Young's modulus and the tensile strength of the system only at low fibres content (Fig. 5).

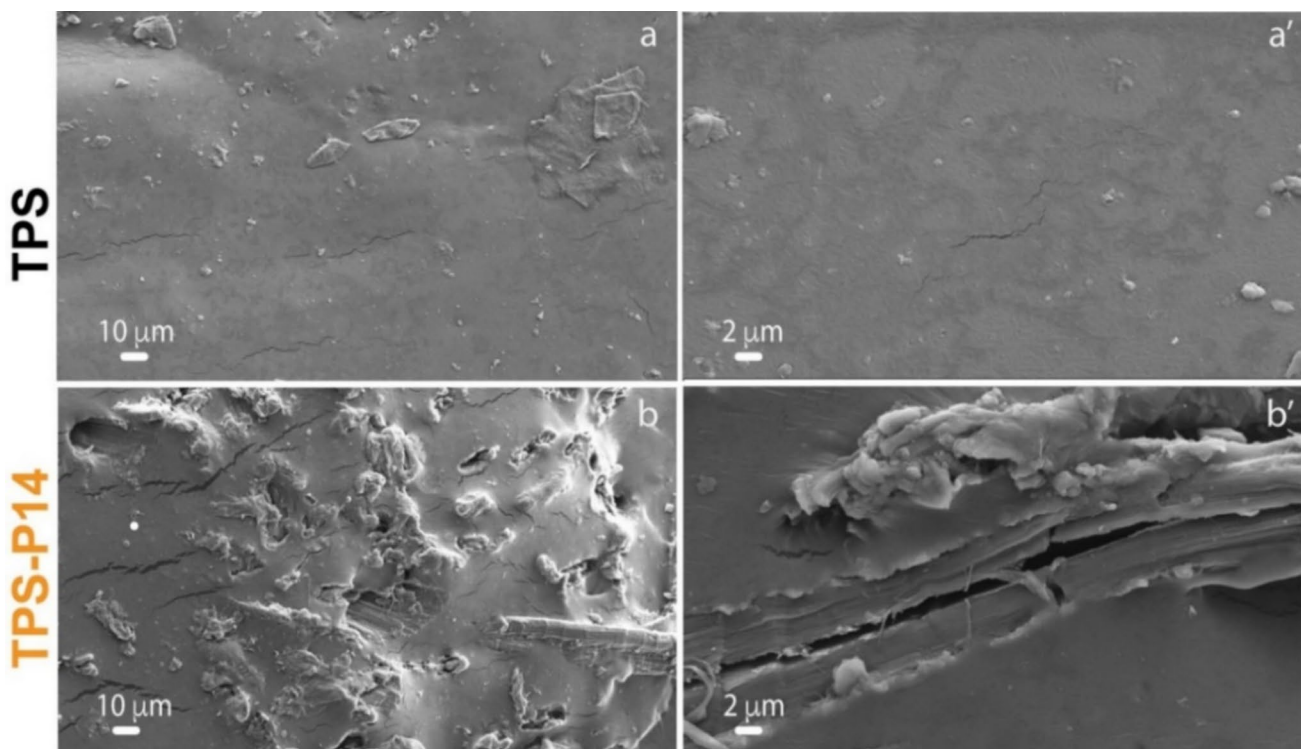


Fig. 4 SEM micrographs of wet TPS (a, a') and TPS-P14 (b, b') cryo-fractured surfaces. Size bars of 10 μm are reported for the low magnified micrographs (a, b), and 2 μm for the high magnified micrographs (a' and b')

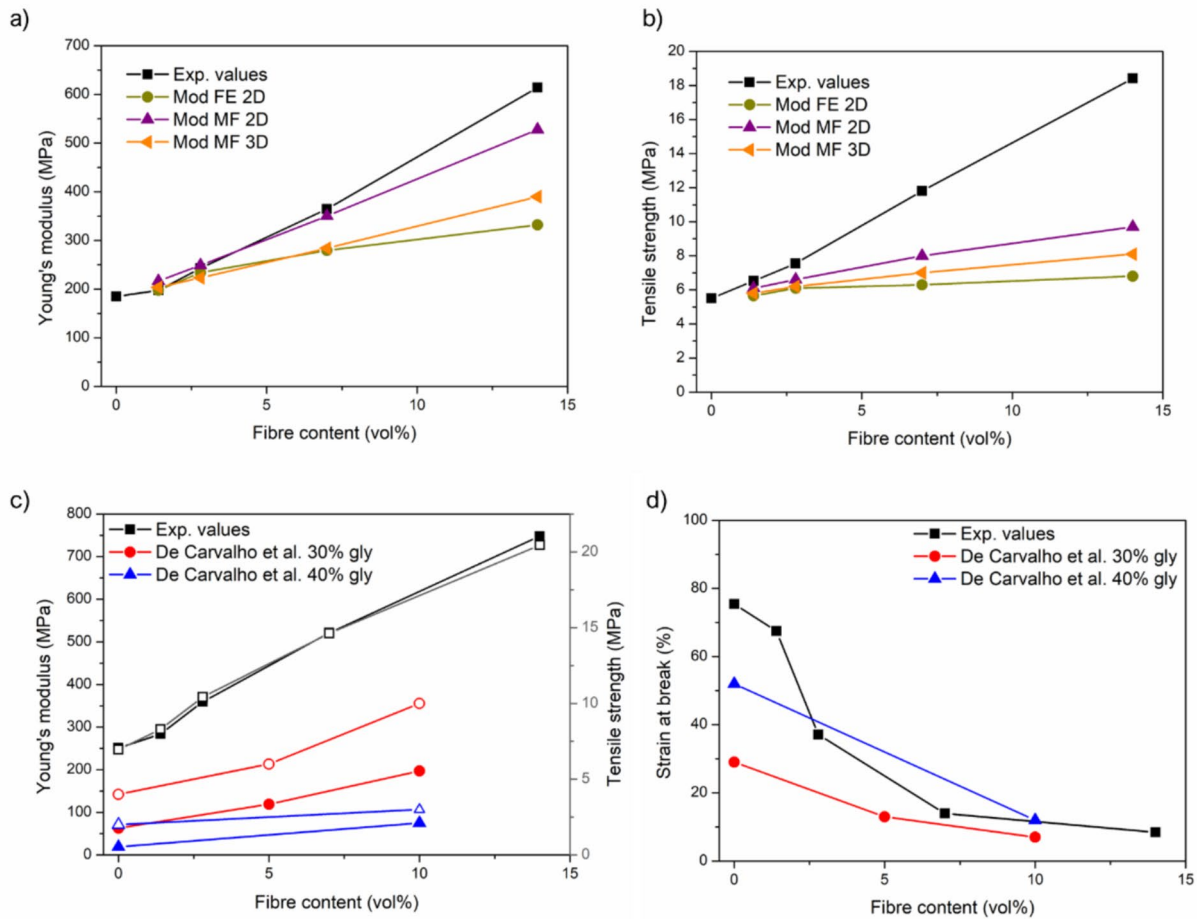


Fig. 5 Young’s moduli (a) and tensile strength (b) as a function of fibres content for the experimental results compared with the modelling values at 10 mm/min. (c) Young’s moduli (black-filled symbols, y-axis on the left) and tensile strength (hollow symbols, y-axis on the

right) and (d) strain at break as a function of fibres content for the experimental results of this work compared with literature values [48] at 50 mm/min

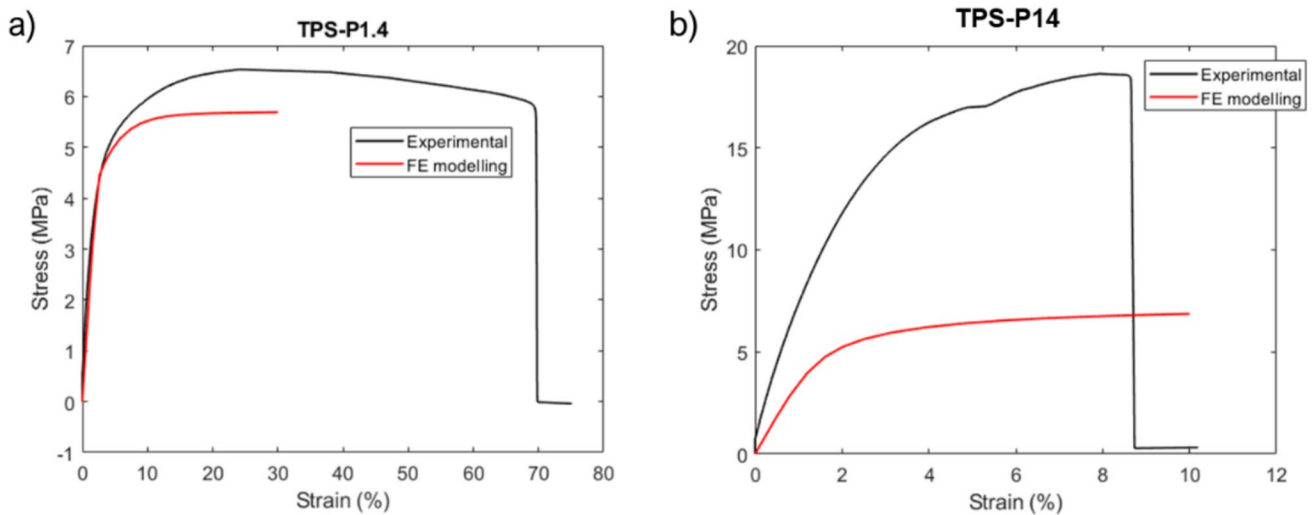


Fig. 6 Comparison of stress–strain curves at 10 mm/min obtained experimentally and by modelling for TPS-P1.4 (a) and TPS-P14 (b)

The tensile curves given by the modelling (FE) have a similar shape to the ones obtained with the real tensile tests (see Fig. 6 and Figs. S6, and S7).

Both FE and MF analysis gave results quite different from the tensile tests, especially for the tensile strength. The random dispersion assumed for the modelling can be one of the reasons for the underestimation of the simulated stiffness and strength compared to the experimental results. It is worth noting that Digimat-MF simulations with all the fibres in the direction of the load were also conducted, and even in this case, the stresses reached were lower than the ones reached experimentally. The discrepancy between the experimental and modelling results increases with the fibres' amount. FE modelling led to lower tensile properties than MF modelling, which resulted in better describing the tensile behaviour of our system for low fibres' content. The prediction of MF can suffer from the design of the RVE that does not capture the properties of the processed materials, which are not merely a combination of the properties of the starting materials, but the result of an alteration induced by the reactive process. It was also observed that when the fibres have a planar distribution (2D modelling), the tensile properties are higher than for the 3D random distribution. In fact, in the case of the 2D random distribution, the loading is assumed to be applied in the plane of the fibres, meaning that they provide a higher contribution to the stiffness and strength of the biocomposite.

It is worth noting that for the modelling in the simulations, a single average fibre length was assumed, and fibre agglomerations were neglected. Mentges et al. [49] developed micromechanical modelling approaches for short fibre composites considering fibre length distributions. The study shows that assuming an average fibre length will result in reasonably accurate predictions when compared with the results that take into account an actual fibre length distribution. Hence, a single fibre length should be considered as a rather suitable assumption for the modelling process. A more accurate material characterisation would be needed to assess and quantify fibre agglomerations and consider these phenomena in the micromechanical modelling process, resulting beyond the scope of the current study. Therefore, we chose as aspect ratio the weight average value of the experimental values assessed for TPS-P7 and TPS-P14 (Table 3) and neglected the fines. These assumptions can contribute to the underestimation of the tensile properties.

The tensile properties experimentally observed were also compared with values collected from the literature for TPS materials with a similar amount of plasticiser and citric acid (CA) for wet TPS and pulp fibres for the biocomposites (Fig. 5c, d). A higher elastic modulus, tensile strength, and elongation at break were observed experimentally compared with the values reported by De Carvalho et al. for wood pulp-based biocomposites obtained without citric acid [48].

A similar trend, with three and six times lower tensile moduli and strength, respectively, was obtained for corn starch TPS reinforced with hemp fibres, displaying a continuous increase in both tensile modulus and ultimate strength, proportional to the amount of reinforcement [50]. Our values are more than three times higher than those of other potato starch-based composites reinforced with natural fillers [51].

Aiming at providing another perspective, we proposed a Finite-Element approach (FEA) that does not consider the microstructural features obtained by the fabrication process but, aiming at devising a simple and effective model able to catch the order of magnitude of the phenomena, employs a perfect adhesion at the interface between fibres and matrix, whose stiffnesses are recalculated based on the elaboration of experimental data with the Nielsen analytical model. Increasing the speed rate of the test the tensile properties of the composites result in higher Young's moduli and tensile strengths (Fig. 5a, b vs. c), as expected for viscoelastic systems. Therefore, we tested our approach on the Young's moduli obtained at a strain rate equal to 50 mm/min (Fig. 7), a case even more challenging to describe than that of 10 mm/min, for which the traditional approach failed to estimate the mechanical behaviour of the composite. As for the interpolation of the experimental data, we chose as analytical functions $f(V_f)$, $g(V_f)$ two polynomial functions since this approximation led to R^2 greater than 0.99. In particular, we obtained the following coefficients for Eq. 3:

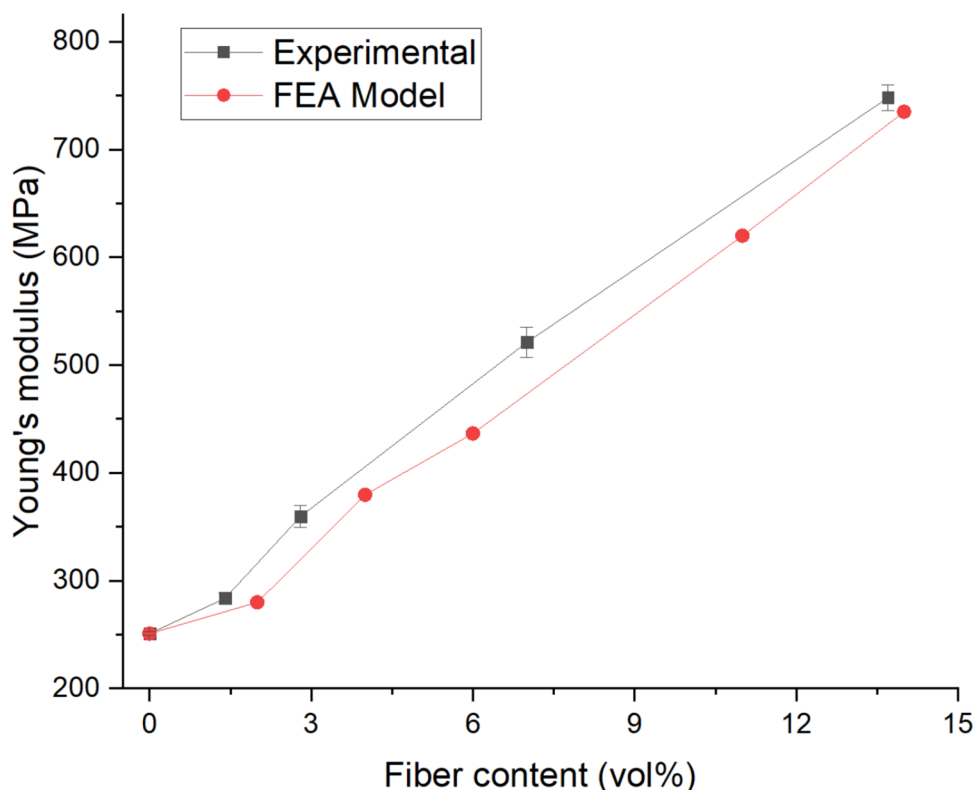
$$f(V_f) : \begin{cases} a = 8.3 \\ b = 30.2 \\ c = -153.1 \end{cases} \quad g(V_f) : \begin{cases} d = 1236 \\ e = -5602 \\ f = 7097 \end{cases} \quad (4)$$

Figure 7 reports the results of the simulations, where it is possible to appreciate how the synergies of FE modelling, experimental data, and analytical model led to a good estimation of the mechanical properties of the composite with a little computational cost with an average error of 10%. On the other hand, the main limitation of such method consists in a preliminary elaboration of the experimental data that might be expensive.

4 Insight on the mechanical reinforcement

As reported in the Modelling section in the Supporting Information (Sect. 7), different assumptions such as random 2D and 3D distribution of fibres, equal fibre lengths, and the absence of agglomerates (among others) were made in the micro-mechanical simulations. One of the most important assumptions in the simulations with traditional modelling approaches is the constant properties of the matrix material

Fig. 7 Results of the synergistic FE model and comparison with the experimental results. The average error between FEA and experimental results is on average about 10%



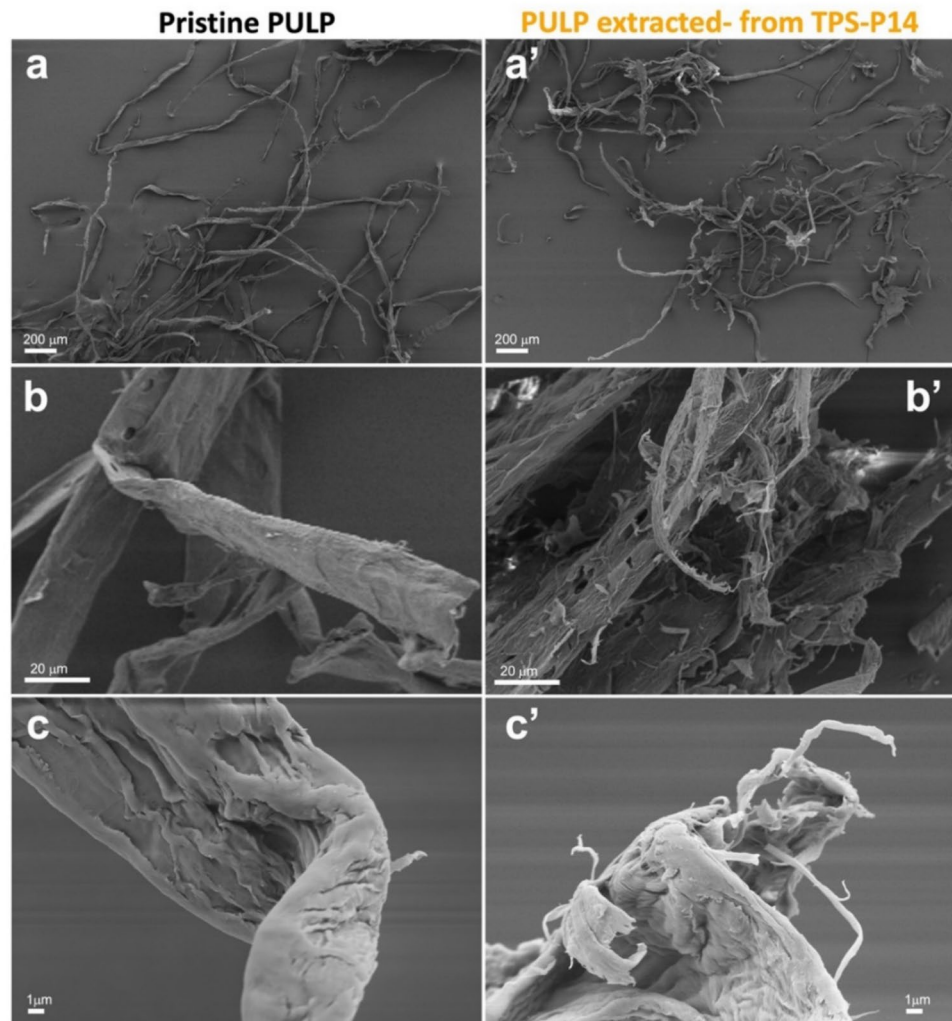
in the entire RVE. This is probably not true for TPS matrices in general, due to the gelatinization process aiming to reduce the crystallinity and large molecular weight of native starch to improve its melt processability. Overall, the thermal field towards the material and shear forces generated during the reactive extrusion affect the degree of dispersion and miscibility between the materials, increasing them and provoking the noticeable difference between the real mechanical behaviour and the estimated one. The addition of water into the formulation before the REx acts as a temporary further plasticiser of the system and reduces shear stress during the extrusion, which results in milder shortening of the fibres in comparison with the dry-fed traditional melt compounding [30]. However, the viscosity of the composites increases with the fibre content, i.e. the materials experience increasing shear stress during compounding at the same processing parameters. This can cause changes in the structures of the starch molecules, such as a decrease in molecular weight, and of the pulp fibres, such as shortening and fibrillation. To qualitatively validate this hypothesis, the morphology of the fibres recovered after Soxhlet extraction from DMSO was investigated (Fig. 8). The fibre shortening was assessed by using a fibre analyser, which indicated a 79 and 88% length reduction for the fibres recovered after Soxhlet extraction from DMSO of TPS-P7 and TPS-P14, respectively, compared to the neat pulp fibres (Table 3). Among the shortening evidence, the larger number of fines (fibres shorter

than 0.02 mm) generated after melt processing detected from the fibre analyser in TPS-P7 and TPS-P14 (7 and 9 times larger than the ones registered for the pristine pulp) is already visible at lower magnification for the observed fibres extracted from TPS-P14 (Fig. 8a, a'). The fibre diameter increases by about 50% after melt processing compared with neat fibres measured by the fibre analyser, attributed to fibrillation (Table 3). The morphological analysis confirms the fibrillation of fibres during melt processing. The fibres recovered from the TPS-P14 sample show thinner micro and nanofibrils shredded (Fig. 8b', c') from the pristine supramolecular organisation shown by the unprocessed pulp fibres (Fig. 8b, c).

Therefore, the changes in the materials' structure during melt processing are responsible for the higher tensile properties of the composites measured experimentally, compared to the ones estimated by the modelling, and those reported for similar composites in the literature. Moreover, reactions between fibres and matrix are ignored in the modelling assumptions, which essentially means that any crosslinking at the interphase is not considered.

Furthermore, the differences between the modelling and experimental values could also be explained by the effect of citric acid and free water in the TPS formulation. As previously reported in the literature, the addition of citric acid could induce both starch hydrolysis and crosslinking. Reddy and Yang [52], for the first time, as well as other authors

Fig. 8 SEM micrography of (a–c) the pristine pulp fibres (unprocessed) and recovered after Soxhlet extraction of the TPS-P14 sample from DMSO (a'–c')



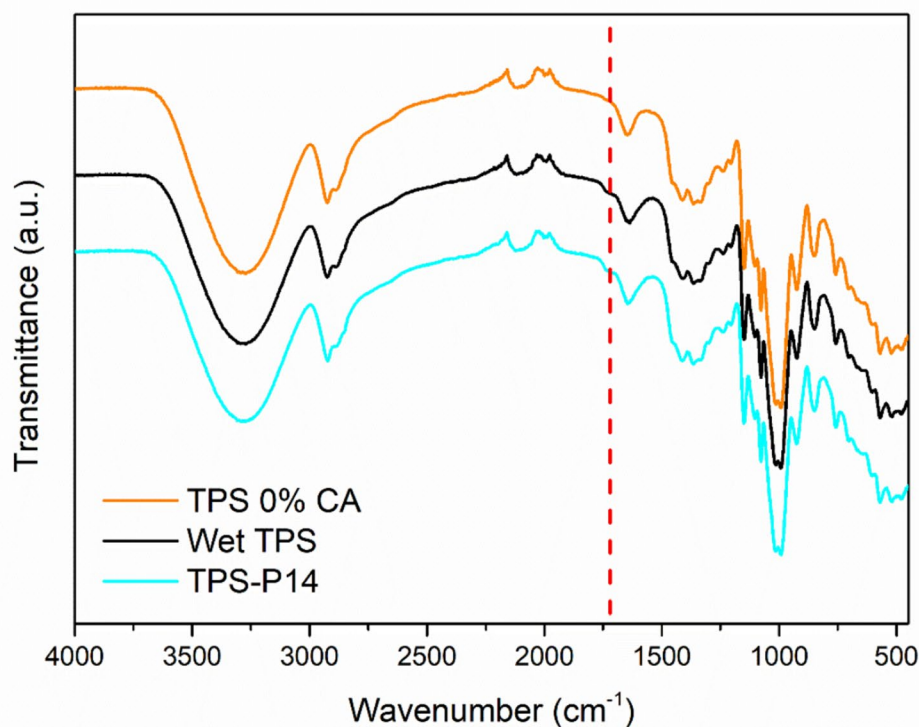
later [53–56], showed that CA allows the crosslinking of starch films, which leads to the improvement of the tensile properties. The pH of the system and the temperature of the processing are critical parameters for the crosslinking reactions. The appearance of the band at 1725–1740 cm^{-1} by Fourier-transform infrared (FTIR) spectroscopy has been considered the major evidence of the chemical process of crosslinking with citric acid [57–59] being ascribed to the carboxyl and ester carbonyl groups. However, the hydrolysis of starch when the pH decreases is a concurrent reaction to crosslinking, provoked by the CA addition. High water content, temperature, and the CA concentration increase the hydrolysis rate [55, 60–63].

To confirm the crosslinking reactions of starch catalysed by the presence of the CA in the formulation, FTIR spectroscopy was performed. FTIR spectra of the TPS with and without the CA, and the TPS-14 presented peaks related to carbohydrate structures (Fig. 9) [57, 64, 65]. In particular, the peaks observed were the bands in the region of 3000–3500 cm^{-1} and 2800–3000 cm^{-1} are ascribed to the

O–H stretching and C–H stretching, respectively. Moreover, the peak observed at 1640 cm^{-1} is attributed to the O–H bending of bounded water, while the peak at 1460 cm^{-1} is assigned to the O–H bending of the starch molecule [57, 63, 64]. A small band appeared around 1740 cm^{-1} indicating the presence of crosslinked starch fraction.

The acid hydrolysis of starch was also confirmed by the Thermogravimetric Analysis (TGA) since a decrease in the onset of degradation was observed for the sample containing the CA compared with native starch (Table S1), as previously reported [66]. The thermal degradation of native starch occurred in a single step at about 305 °C because of oxidation and subsequent scission of starch chains, leaving 22% of char (Fig. S9 and Table S1), as previously reported. Likewise, pristine pulp fibre thermal degradation occurred in one step at 356 °C, showing 24% of the chart left (Fig. S9 and Table S1). The thermal decomposition of wet TPS and its biocomposites occurred in three main steps. The first step, around 145 °C, is due to dehydration, and the second step between 210 and 290 °C is probably due to the

Fig. 9 FTIR spectra of TPS (with and without CA) and TPS-P14 comparison



decomposition of the glycerol-rich phase. All the samples showed a peak around 250 °C or slightly lower, unless TPS-P14 showed a peak about 280 °C. This shift towards higher temperature is probably due to the higher interaction of starch with glycerol when not inhibited by free water added into the formulation, as for the other samples, leading to a more efficient starch plasticisation for TPS-P14, and consistent with the reduction in the TPS-P14's T_g commented in DMTA analysis (Sect. 4 in Supporting Information). Finally, the third step is due to the oxidation of partially decomposed starch at about 320 °C, while the last shoulder at around 355 °C is due to the pulp fibres thermal degradation, as reported from other authors [67]. It is worth noticing that even after the reactive melt processing, the thermal stability of pulp fibres remained unchanged. On the other hand, other authors reported that the thermal decomposition observed below 290 °C could be related to the free glycerol-rich phase and esterified glycerol molecules associated with the more unstable ether linkages formed between the CA and glycerol [62] and to the hydrolysed starch chains [52, 53, 64]. Confirming this hypothesis, the decrease of char percentage observed for wet TPS compared to that of native starch supports the chain scission of the starch during the melt processing.

Based on the above reported results presented, we may conclude that the CA can serve as a co-plasticiser in the plasticization process of starch, establishing a balance

between the processability and the tensile properties of TPS as previously reported [62]. Moreover, the induced hydrolysis can lead to the shortening of the starch, generating a higher amount of hydroxyl moieties that can migrate faster towards the pulp fibres at the interphase region and form a higher level of hydrogen bonding. These strong interactions between the polymeric matrix and the pulp fibres are consistent with the morphological analysis and the increase in tensile properties as the amount of the pulp fibres increases. Moreover, the detected improved fibres/TPS interphase interactions support the more effective fibres dispersion within the polymer matrix.

Our modelling approach aimed at describing this intriguing mechanical performance through a simplified macroscale model based on the experimental results, and that could be used for further speculations on the effects of different compositions.

In order to reduce the gap between the experimental and modelling results, a multiscale approach on the mechanochemical mechanisms at the filler-matrix interface would be required to deeply investigate the effects of the reactive extrusion on the surface chemistry of the interface. This methodology, however, would require a dedicated *in silico* study that, although of high interest, goes beyond the scope of this paper, which serves as a motivation for further investigation.

5 Conclusions

In this study, we successfully designed a single-step reactive extrusion assisted by water to obtain biocomposites with outstanding mechanical properties and proposed a combination of experimental and modelling for the understanding of the reinforcement mechanism.

Our results support the occurrence of reactive compounding for the starch/pulp fibres biocomposites. Experiments and computational modelling of the plasticized starch and its biocomposites with the pulp fibres were investigated and compared. The deviation between the actual and simulated results has levered the scrutiny of the reinforcement mechanism, where traditional modelling hypotheses failed to describe the system, i.e. at the matrix/fibres interface. Structural and morphological results confirmed that the reason for the experiment/traditional modelling discrepancy lies in the improved fibres/TPS interface obtained by the designed reactive extrusion approach, which overcomes the traditional concept of perfect adhesion and highlights the limit of modelling to estimate the tensile properties of the biocomposites.

The morphological evidence of improved dispersion and cohesive fracture propagation within the fibre structure confirms that the inherent hypotheses of the description of the system fail when the biocomposites are reactive compounded. The perfect adhesion at the TPS/fibres interphase after the reactive compounding is too restrictive to efficiently describe the system properties, which instead are improved due to a change of the pristine TPS and fibre properties. The reactive extrusion approach leads to an improved interphase region due to dispersion/fibrillation of the fibres within the TPS matrix ascribed to an improved stress transfer due to a larger surface contact between the fibres and the thermoplastic starch. Overall, the experimental/simulation discrepancy indicates a clear need for a more performant modelling design in the description of reactively prepared biocomposites. Because of this, we proposed a different but effective modelling approach that synergistically considers the experimental data and analytical model despite requiring a preliminary elaboration of the materials' properties. This novel toolbox enables the description of the phenomena at the reactive extruded interface via an artefact of a mechanical mechanism in composites using a traditional FE simulation, avoiding computationally expensive molecular dynamics studies, not limited to our specific set of data.

Further investigations on a more efficient modelling description of the mechanics of the interface are still required, and this is the research avenue where our effort is currently focused.

Supplementary Information The online version contains supplementary material available at <https://doi.org/10.1007/s42114-025-01460-5>.

Author contributions Author contribution to the manuscript Valentina Sessini: Investigation, Data curation, Formal analysis, Validation, Visualization, Writing- Original draft preparation, Writing-reviewing, and editing. Hélène Latty: Formal analysis, Investigation. Mario Milazzo: Conceptualization, Methodology, Formal analysis, Validation, Writing-reviewing and editing. Mohsen Mirkhalaf: Software, Supervision, Writing-reviewing and editing. Funding acquisition. Giada Lo Re: Conceptualization, Methodology, Formal analysis, Validation, Writing-reviewing and editing. Supervision, Resources, Project administration, Funding acquisition.

Funding Open access funding provided by Chalmers University of Technology. GLR acknowledges the BioInnovation ProDAC (grant number 2021-02094) and the Wallenberg Wood Science Centre (WWSC) 3.0 program for the financial support. Mohsen Mirkhalaf gratefully acknowledges financial support from the Vetenskapsrådet, Sweden (Swedish Research Council, VR grant number: 2019-04715).

Data availability All data will be made available on request.

Declarations

Competing interests The authors declare no competing interests.

Open Access This article is licensed under a Creative Commons Attribution 4.0 International License, which permits use, sharing, adaptation, distribution and reproduction in any medium or format, as long as you give appropriate credit to the original author(s) and the source, provide a link to the Creative Commons licence, and indicate if changes were made. The images or other third party material in this article are included in the article's Creative Commons licence, unless indicated otherwise in a credit line to the material. If material is not included in the article's Creative Commons licence and your intended use is not permitted by statutory regulation or exceeds the permitted use, you will need to obtain permission directly from the copyright holder. To view a copy of this licence, visit <http://creativecommons.org/licenses/by/4.0/>.

References

1. Khalid MY, Arif ZU (2022) Novel biopolymer-based sustainable composites for food packaging applications: a narrative review. *Food Packaging Shelf* 33:100892. <https://doi.org/10.1016/j.fpsl.2022.100892>
2. Explained ES (2023) Packaging waste statistics https://ec.europa.eu/eurostat/statistics-explained/index.php?title=Packaging_waste_statistics#Waste_generation_by_packaging_material. Accessed 24 Feb 2025
3. Song JH, Murphy RJ, Narayan R, Davies GBH (2009) Biodegradable and compostable alternatives to conventional plastics. *Philos Trans R Soc Lond B Biol Sci* 364(1526):2127–2139. <https://doi.org/10.1098/rstb.2008.0289>
4. Westlake JR, Tran MW, Jiang Y, Zhang X, Burrows AD, Xie M (2023) Biodegradable biopolymers for active packaging: demand, development and directions. *Sustain Food Technol* 1(1):50–72. <https://doi.org/10.1039/D2FB00004K>
5. European Bioplastics n-I (2022) Bioplastics market data. <https://www.european-bioplastics.org/market/>. Accessed 24 Feb 2025
6. Aleksanyan KV (2023) Polysaccharides for biodegradable packaging materials: past, present, and future (brief review). *Polymers* 15(2):451. <https://doi.org/10.3390/polym15020451>

7. Surendren A, Mohanty AK, Liu Q, Misra M (2022) A review of biodegradable thermoplastic starches, their blends and composites: recent developments and opportunities for single-use plastic packaging alternatives. *Green Chem* 24(22):8606–8636. <https://doi.org/10.1039/D2GC02169B>
8. Sessini V, Raquez J-M, Lourdin D, Maigret J-E, Kenny JM, Dubois P, Peponi L (2017) Humidity-activated shape memory effects on thermoplastic starch/EVA blends and their compatibilized nanocomposites. *Macromol Chem Phys* 218(24):1700388. <https://doi.org/10.1002/macp.201700388>
9. Serra-Parareda F, Delgado-Aguilar M, Espinach FX, Mutjé P, Boufi S, Tarrés Q (2022) Sustainable plastic composites by polylactic acid-starch blends and bleached kraft hardwood fibers. *Compos Part B-Eng* 238:109901. <https://doi.org/10.1016/j.compositesb.2022.109901>
10. Samir A, Ashour FH, Hakim AAA, Bassyouni M (2022) Recent advances in biodegradable polymers for sustainable applications. *npj Mater Degrad* 6(1):68. <https://doi.org/10.1038/s41529-022-00277-7>
11. Kazayawoko M, Balatinecz JJ, Matuana LM (1999) Surface modification and adhesion mechanisms in woodfiber-polypropylene composites. *J Mater Sci* 34(24):6189–6199. <https://doi.org/10.1023/A:1004790409158>
12. Mohanty AK, Vivekanandhan S, Pin J-M, Misra M (2018) Composites from renewable and sustainable resources: challenges and innovations. *Science* 362(6414):536–542. <https://doi.org/10.1126/science.aat9072>
13. Raj RG, Kokta BV, Daneault C (1989) Effect of chemical treatment of fibers on the mechanical properties of polyethylene-wood fiber composites. *J Adhes Sci Technol* 3(1):55–64. <https://doi.org/10.1163/156856189X00056>
14. Pickering KL, Efendy MGA, Le TM (2016) A review of recent developments in natural fibre composites and their mechanical performance. *Compos Part A-Appl S* 83:98–112. <https://doi.org/10.1016/j.compositesa.2015.08.038>
15. Belgacem MN, Gandini A (2005) The surface modification of cellulose fibres for use as reinforcing elements in composite materials. *Compos Interfaces* 12(1–2):41–75. <https://doi.org/10.1163/1568554053542188>
16. Bledzki AK, Gassan J (1999) Composites reinforced with cellulose based fibres. *Prog Polym Sci* 24(2):221–274. [https://doi.org/10.1016/S0079-6700\(98\)00018-5](https://doi.org/10.1016/S0079-6700(98)00018-5)
17. Belgacem MN, Bataille P, Sapieha S (1994) Effect of corona modification on the mechanical properties of polypropylene/cellulose composites. *J Appl Polym Sci* 53(4):379–385. <https://doi.org/10.1002/app.1994.070530401>
18. Fazeli M, Florez JP, Simão RA (2019) Improvement in adhesion of cellulose fibers to the thermoplastic starch matrix by plasma treatment modification. *Compos Part B-Eng* 163:207–216. <https://doi.org/10.1016/j.compositesb.2018.11.048>
19. Miao C, Hamad WY (2013) Cellulose reinforced polymer composites and nanocomposites: a critical review. *Cellulose* 20(5):2221–2262. <https://doi.org/10.1007/s10570-013-0007-3>
20. Morales J, Olayo MG, Cruz GJ, Herrera-Franco P, Olayo R (2006) Plasma modification of cellulose fibers for composite materials. *J Appl Polym Sci* 101(6):3821–3828. <https://doi.org/10.1002/app.24085>
21. Lo Re G, Engström J, Wu Q, Malmström E, Gedde UW, Olsson RT, Berglund L (2018) Improved cellulose nanofibril dispersion in melt-processed polycaprolactone nanocomposites by a latex-mediated interphase and wet feeding as LDPE alternative. *ACS Appl Nano Mater* 1(6):2669–2677. <https://doi.org/10.1021/acsnm.8b00376>
22. Saedi S, Garcia CV, Kim JT, Shin GH (2021) Physical and chemical modifications of cellulose fibers for food packaging applications. *Cellulose* 28(14):8877–8897. <https://doi.org/10.1007/s10570-021-04086-0>
23. Spoljaric S, Genovese A, Shanks RA (2009) Polypropylene-microcrystalline cellulose composites with enhanced compatibility and properties. *Compos Part A-Appl S* 40(6):791–799. <https://doi.org/10.1016/j.compositesa.2009.03.011>
24. Chen P, Lo Re G, Berglund LA, Wohler J (2020) Surface modification effects on nanocellulose – molecular dynamics simulations using umbrella sampling and computational alchemy. *J Mater Chem A* 8(44):23617–23627. <https://doi.org/10.1039/D0TA09105G>
25. Cichosz S, Masek A, Rylski A (2020) Cellulose modification for improved compatibility with the polymer matrix: mechanical characterization of the composite material. *Materials* 13(23):5519. <https://doi.org/10.3390/ma13235519>
26. Lo Re G, Spinella S, Boujemaoui A, Vilaseca F, Larsson PT, Adås F, Berglund LA (2018) Poly(ϵ -caprolactone) biocomposites based on acetylated cellulose fibers and wet compounding for improved mechanical performance. *ACS Sustain Chem Eng* 6(5):6753–6760. <https://doi.org/10.1021/acssuschemeng.8b00551>
27. Magnani C, Idström A, Nordstierna L, Müller AJ, Dubois P, Raquez J-M, Lo Re G (2020) Interphase design of cellulose nanocrystals/poly(hydroxybutyrate-ran-valerate) bionanocomposites for mechanical and thermal properties tuning. *Biomacromolecules* 21(5):1892–1901. <https://doi.org/10.1021/acs.biomac.9b01760>
28. Spinella S, Lo Re G, Liu B, Dorgan J, Habibi Y, Leclère P, Raquez J-M, Dubois P, Gross RA (2015) Polylactide/cellulose nanocrystal nanocomposites: efficient routes for nanofiber modification and effects of nanofiber chemistry on PLA reinforcement. *Polymer* 65:9–17. <https://doi.org/10.1016/j.polymer.2015.02.048>
29. Dubois P (2022) Reactive extrusion (REX): using chemistry and engineering to solve the problem of Ocean plastics. *Engineering* 14:15–18. <https://doi.org/10.1016/j.eng.2021.12.009>
30. Lo Re G, Sessini V (2018) Wet feeding approach for cellulosic materials/PCL biocomposites, biomass extrusion and reaction technologies: principles to practices and future potential, *American Chemical Society*, pp. 209–226. <https://doi.org/10.1021/bk-2018-1304.ch011>
31. Lv S, Gu J, Tan H, Zhang Y (2016) Modification of wood flour/PLA composites by reactive extrusion with maleic anhydride. *J Appl Polym Sci* 133(15):43295. <https://doi.org/10.1002/app.43295>
32. Venkatesh A, Forsgren L, Avella A, Banke K, Wahlberg J, Vilaseca F, Lo Re G, Boldizar A (2022) Water-assisted melt processing of cellulose biocomposites with poly(ϵ -caprolactone) or poly(ethylene-acrylic acid) for the production of carton screw caps. *J Appl Polym Sci* 139(6):51615. <https://doi.org/10.1002/app.51615>
33. Zhai X, Wang W, Zhang H, Dai Y, Dong H, Hou H (2020) Effects of high starch content on the physicochemical properties of starch/PBAT nanocomposite films prepared by extrusion blowing. *Carbohydr Polym* 239:116231. <https://doi.org/10.1016/j.carbpol.2020.116231>
34. Lu Q, Zograf G (1997) Properties of citric acid at the glass transition. *J Pharm Sci* 86(12):1374–1378. <https://doi.org/10.1021/js970157y>
35. Oliveira MLN, Malagani RA, Franco MR (2013) Solubility of citric acid in water, ethanol, n-propanol and in mixtures of ethanol+water. *Fluid Phase Equilib* 352:110–113. <https://doi.org/10.1016/j.fluid.2013.05.014>
36. Ogierman W, Kokot G (2013) Mean field homogenization in multi-scale modelling of composite materials. *J Achiev Mater Manuf Eng* 61(2):343–348. http://jamme.acmsse.h2.pl/papers_vol61_2/6152.pdf

37. Sliseris J, Yan L, Kasal B (2016) Numerical modelling of flax short fibre reinforced and flax fibre fabric reinforced polymer composites. *Compos Part B-Eng* 89:143–154. <https://doi.org/10.1016/j.compositesb.2015.11.038>
38. Tikarrouchine E, Chatzigeorgiou G, Praud F, Piotrowski B, Chemisky Y, Meraghni F (2018) Three-dimensional FE2 method for the simulation of non-linear, rate-dependent response of composite structures. *Compos Struct* 193:165–179. <https://doi.org/10.1016/j.compstruct.2018.03.072>
39. Mirkhalaf SM, Eggels EH, Van Beurden TJH, Larsson F, Fagerström M (2020) A finite element based orientation averaging method for predicting elastic properties of short fiber reinforced composites. *Compos Part B-Eng* 202:108388. <https://doi.org/10.1016/j.compositesb.2020.108388>
40. Mirkhalaf SM, van Beurden TJH, Ekh M, Larsson F, Fagerström M (2022) An FE-based orientation averaging model for elasto-plastic behavior of short fiber composites. *Int J Mech Sci* 219:107097. <https://doi.org/10.1016/j.ijmecsci.2022.107097>
41. Loos M (2015) Chapter 5 - Fundamentals of polymer matrix composites containing CNTs. In: Loos M (ed) *Carbon Nanotube Reinforced Composites*. William Andrew Publishing, Oxford, pp 125–170
42. Sessini V, Haseeb B, Boldizar A, Re GL (2021) Sustainable pathway towards large scale melt processing of the new generation of renewable cellulose–polyamide composites. *RSC Adv* 11(2):637–656. <https://doi.org/10.1039/D0RA07141B>
43. Róz ALD, Carvalho AJF, Gandini A, Curvelo AAS (2006) The effect of plasticizers on thermoplastic starch compositions obtained by melt processing. *Carbohydr Polym* 63(3):417–424. <https://doi.org/10.1016/j.carbpol.2005.09.017>
44. Sessini V, Raquez J-M, Lo Re G, Mincheva R, Kenny JM, Dubois P, Peponi L (2016) Multiresponsive shape memory blends and nanocomposites based on starch. *ACS Appl Mater Interfaces* 8(30):19197–19201. <https://doi.org/10.1021/acsami.6b06618>
45. Lafargue D, Pontoire B, Buléon A, Doublier JL, Lourdin D (2007) Structure and mechanical properties of hydroxypropylated starch films. *Biomacromol* 8(12):3950–3958. <https://doi.org/10.1021/bm7009637>
46. Lopez-Rubio A, Flanagan BM, Gilbert EP, Gidley MJ (2008) A novel approach for calculating starch crystallinity and its correlation with double helix content: a combined XRD and NMR study. *Biopolymers* 89(9):761–768. <https://doi.org/10.1002/bip.21005>
47. Sessini V, Arrieta MP, Kenny JM, Peponi L (2016) Processing of edible films based on nanoreinforced gelatinized starch. *Polym Degrad Stab* 132:157–168. <https://doi.org/10.1016/j.polyimdegradstab.2016.02.026>
48. De Carvalho AJF, Curvelo AAS, Agnelli JAM (2002) Wood pulp reinforced thermoplastic starch composites. *Int J Polym Mater* 51(7):647–660. <https://doi.org/10.1080/714975803>
49. Mentges N, Çelik H, Hopmann C, Fagerström M, Mirkhalaf SM (2023) Micromechanical modelling of short fibre composites considering fibre length distributions. *Compos Part B Eng* 264:110868. <https://doi.org/10.1016/j.compositesb.2023.110868>
50. Gironès J, López JP, Mutjé P, Carvalho AJF, Curvelo AAS, Vilaseca F (2012) Natural fiber-reinforced thermoplastic starch composites obtained by melt processing. *Compos Sci Technol* 72(7):858–863. <https://doi.org/10.1016/j.compscitech.2012.02.019>
51. Bénézét JC, Stanojlovic-Davidovic A, Bergeret A, Ferry L, Crespy A (2012) Mechanical and physical properties of expanded starch, reinforced by natural fibres. *Ind Crops Prod* 37(1):435–440. <https://doi.org/10.1016/j.indcrop.2011.07.001>
52. Reddy N, Yang Y (2010) Citric acid cross-linking of starch films. *Food Chem* 118(3):702–711. <https://doi.org/10.1016/j.foodchem.2009.05.050>
53. Chen WC, Judah SNMSM, Ghazali SK, Munthoub DI, Alias H, Mohamad Z, Majid RA (2021) The effects of citric acid on thermal and mechanical properties of crosslinked starch film. *Chem Eng Trans* 83:199–204. <https://doi.org/10.3303/CET2183034>
54. Menzel C (2020) Improvement of starch films for food packaging through a three-principle approach: antioxidants, cross-linking and reinforcement. *Carbohydr Polym* 250:116828. <https://doi.org/10.1016/j.carbpol.2020.116828>
55. Menzel C, Olsson E, Plivelic TS, Andersson R, Johansson C, Kuktaita R, Järnström L, Koch K (2013) Molecular structure of citric acid cross-linked starch films. *Carbohydr Polym* 96(1):270–276. <https://doi.org/10.1016/j.carbpol.2013.03.044>
56. Seligra PG, Medina Jaramillo C, Fama L, Goyanes S (2016) Biodegradable and non-retrogradable eco-films based on starch-glycerol with citric acid as crosslinking agent. *Carbohydr Polym* 138:66–74. <https://doi.org/10.1016/j.carbpol.2015.11.041>
57. Duarte GA, Bezerra MC, Bettini SHP, Lucas AA (2023) Real-time monitoring of the starch cross-linking with citric acid by chemorheological analysis. *Carbohydr Polym* 311:120733. <https://doi.org/10.1016/j.carbpol.2023.120733>
58. Gerezgiher AG, Szabó T (2022) Crosslinking of starch using citric acid. *J Phys Conf Ser* 2315(1):012036. <https://doi.org/10.1088/1742-6596/2315/1/012036>
59. Lipatova IM, Yusova AA (2021) Effect of mechanical activation on starch crosslinking with citric acid. *Int J Biol Macromol* 185:688–695. <https://doi.org/10.1016/j.ijbiomac.2021.06.139>
60. Carvalho AJF, Zambon MD, da Silva Curvelo AA, Gandini A (2005) Thermoplastic starch modification during melt processing: hydrolysis catalyzed by carboxylic acids. *Carbohydr Polym* 62(4):387–390
61. Chabrat E, Abdillahi H, Rouilly A, Rigal L (2012) Influence of citric acid and water on thermoplastic wheat flour/poly(lactic acid) blends. I: Thermal, mechanical and morphological properties. *Ind Crop Prod* 37(1):238–246. <https://doi.org/10.1016/j.indcrop.2011.11.034>
62. Javid Z, Nazockdast H, Ghasemi I (2021) Unraveling the effect of citric acid on microstructure, rheology, and structural recovery of thermoplastic potato starch. *Starch-Stärke* 73(5–6):2000193. <https://doi.org/10.1002/star.202000193>
63. Olsson E, Menzel C, Johansson C, Andersson R, Koch K, Järnström L (2013) The effect of pH on hydrolysis, cross-linking and barrier properties of starch barriers containing citric acid. *Carbohydr Polym* 98(2):1505–1513. <https://doi.org/10.1016/j.carbpol.2013.07.040>
64. Prachayawarakorn J, Tamseekham J (2019) Chemical modification of biodegradable cassava starch films by natural mono-, di- and tri-carboxylic acids. *Songklanakarin J Sci Technol* 41(2):355–362
65. Sessini V, Arrieta MP, Raquez J-M, Dubois P, Kenny JM, Peponi L (2019) Thermal and composting degradation of EVA/thermoplastic starch blends and their nanocomposites. *Polym Degrad Stab* 159:184–198. <https://doi.org/10.1016/j.polyimdegradstab.2018.11.025>
66. Jiugao Y, Ning W, Xiaofei M (2005) The effects of citric acid on the properties of thermoplastic starch plasticized by glycerol. *Starch-Stärke* 57(10):494–504. <https://doi.org/10.1002/star.20050423>
67. Sridhara PK, Vilaseca F (2020) Assessment of fiber orientation on the mechanical properties of PA6/cellulose composite. *Appl Sci* 10(16):5565. <https://doi.org/10.3390/app10165565>